

Mechanical formulations for bilinear and trilinear hysteretic models used in base isolators

Athanasios A. Markou¹ · George D. Manolis¹

Received: 15 May 2016 / Accepted: 18 September 2016 / Published online: 30 September 2016
© Springer Science+Business Media Dordrecht 2016

Abstract The best known model for numerically simulating the hysteretic behavior of various structural components is the bilinear hysteretic system. There are two possible mechanical formulations that correspond to the same bilinear model from a mathematical viewpoint. The first one consists of a linear elastic spring connected in series with a parallel system comprising a plastic slider and a linear elastic spring, while the second one comprises a linear elastic spring connected in parallel with an elastic-perfectly plastic system. However, the bilinear hysteretic model is unable to describe either softening or hardening effects in these components. In order to account for this, the bilinear model is extended to a trilinear one. Thus, two trilinear hysteretic models are developed and numerically tested, and the analysis shows that both exhibit three plastic phases. More specifically, the first system exhibits one elastic phase, while the second one exhibits two elastic phases according to the level of strain amplitude. Next, the change of slope between the plastic phases in unloading does not occur at the same displacement level in the two models. Furthermore, the dissipated energy per cycle in the first trilinear model, as proven mathematically and explained physically, decreases in the case of hardening and increases in the case of softening, while in the second trilinear model the dissipated energy per cycle remains unchanged, as is the case with the bilinear model. Numerical examples are presented to quantify the aforementioned observations made in reference to the mechanical behavior of the two trilinear hysteretic models. Finally, a set of cyclic shear tests over a wide range of strain amplitudes on a high damping rubber bearing is used in the parameter identification of the two different systems, namely (a) trilinear hysteretic models of the first type connected in parallel, and (b) trilinear hysteretic models of the second type also connected in parallel. The results show that the complex nonlinear shear behavior of high

✉ Athanasios A. Markou
athanasiosmarkou@gmail.com

George D. Manolis
gdm@civil.auh.gr

¹ Laboratory for Statics and Dynamics, Department of Civil Engineering, Aristotle University, 54124 Thessaloniki, Greece

damping rubber bearings can be correctly simulated by a parallel system which consists of only one component, namely the trilinear hysteretic system of the first type. The second parallel system was not able to describe the enlargement of the dissipated hysteresis area for large strain amplitudes.

Keywords Bilinear hysteretic model · Trilinear hysteretic model · Hardening effect · Softening effect · Base isolation · High damping rubber bearings

1 Introduction

Material behavior that can be modeled by elementary mechanical systems comprises: (i) elasticity described by a spring, (ii) time-independent plasticity described by a plastic slider and (iii) viscosity described by a dashpot, see Besson et al. (2010). The simplest model to describe the time-independent hysteretic behavior of materials is the bilinear hysteretic model (BHM), which has been used for decades now and combines springs with a plastic slider. In addition to the BHM, smooth hysteretic models exist, such as those proposed by Ozdemir (1976) and by Wen (1976). There are also two sub-formulations for the mechanical behavior of BHM, which correspond to the same basic mathematical representation, see Iwan (1961), Oliveto et al. (2014). More specifically, materials like high damping rubber bearings (HDRBs) exhibit hardening behavior at large strain amplitudes. In order to account for these kind of effects, an extension of the BHM is suggested by using the trilinear hysteretic model (THM), see Tsopelas et al. (1994), Markou and Manolis (2016a), Markou et al. (2016). Apart from use for the simulation of the shear behavior of HDRBs, the THMs have been used also for the simulation of the shear behavior of single, double and triple friction pendulums, as well as for partition wall elements, see Ray et al. (2013), Ray and Reinhorn (2013). There are also mathematical models for describing complex nonlinear behavior of steel, wood and concrete components, but the relevant mechanical models are not clearly defined, see Ibarra et al. (2005). The present work investigates two possible extensions of the THM mechanical representations, to account for either hardening or softening behavior and highlights their differences. To this end, a set of cyclic shear tests on a spare HDRB from the Solarino base isolation project completed in the 2000s (Markou et al. 2014) are used in order to validate and subsequently compare the different type of models in terms of their accuracy.

2 Mechanical formulations for bilinear and trilinear hysteretic models

A BHM can be built using either of two different mechanical formulations, namely the BHM1 and BHM2, see Figs. 1 and 2, respectively. More specifically, BHM1 consists of a linear elastic spring of stiffness k_e^{m1} (element 1) connected in series with a parallel system, i.e., a plastic slider with characteristic force f_s^{m1} (element 2) and a linear elastic spring of stiffness k_{h1}^{m1} (element 3), (see Oliveto et al. 2014), see Fig. 1. Next, BHM2 consists of an elastic-perfectly plastic system connected in parallel with a linear elastic spring of stiffness k_{h1}^{m2} (element 3), (see Iwan 1961), see Fig. 2. The elastoplastic system itself consists of a linear elastic spring of stiffness $(k_e^{m2} - k_{h1}^{m2})$ (element 1) connected in series with a plastic slider with characteristic force f_s^{m2} (element 2). Both models can evolve into 3-parameter

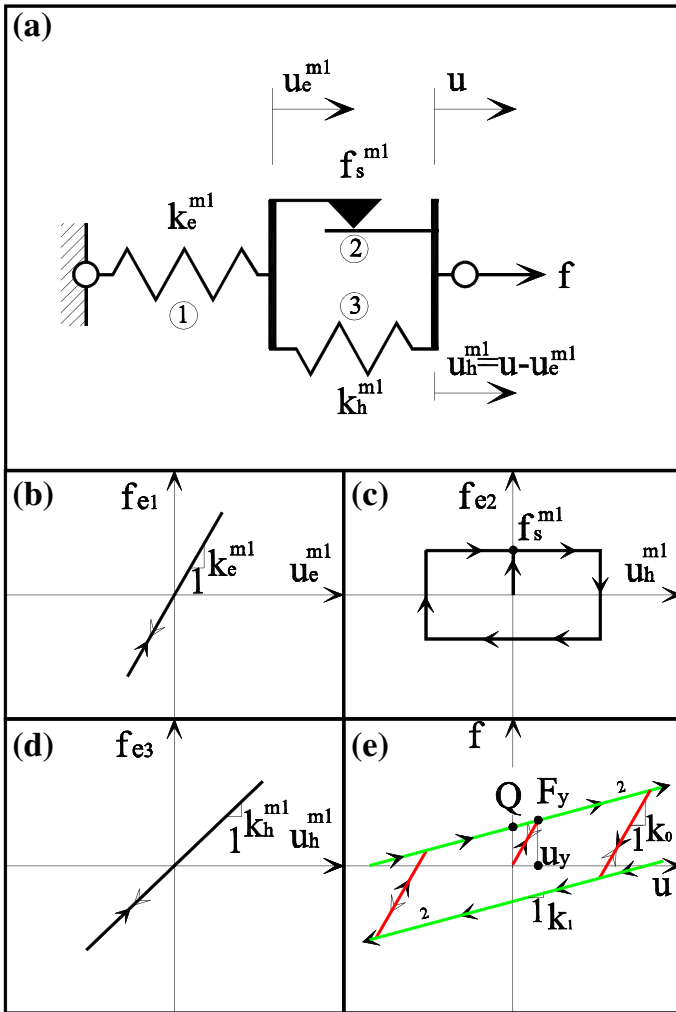


Fig. 1 Bilinear hysteretic model labeled BHM1: **a** mechanical model **b** $f_{e1}-u_e^{m1}$ graph of element 1 **c** $f_{e2}-u_h^{m1}$ graph of element 2 **d** $f_{e3}-u_h^{m1}$ graph of element 3 and **e** overall $f-u$ graph

systems (see Markou et al. 2016) and represent the same mathematical model shown in Figs. 1 and 2.

The extension of both BHMs to their respective THMs is implemented by replacing element 3 with a trilinear elastic spring, see Figs. 3 and 4. In the case of THM1, see Markou and Manolis (2016a), Markou et al. (2016), the parameters needed to describe the trilinear elastic spring (element 3) are the stiffnesses k_{h1}^{m1} , k_{h2}^{m1} and the characteristic displacement u_c^{m1} , see Fig. 3. The positive displacement u_c^{m1} denotes the change of slope in the spring from k_{h1}^{m1} to k_{h2}^{m1} and vice versa for positive displacements u_h^{m1} , while the negative displacement $-u_c^{m1}$ denotes the change of slope between k_{h1}^{m1} and k_{h2}^{m1} , for negative displacements u_h^{m1} . In the case of THM2, see Tsopeles et al. (1994), the three-parameter trilinear spring (element 3) is described by stiffnesses k_{h1}^{m2} , k_{h2}^{m2} and characteristic displacement u_c^{m2} , see Fig. 4. As in the previous case, a positive displacement u_c^{m2} denotes the

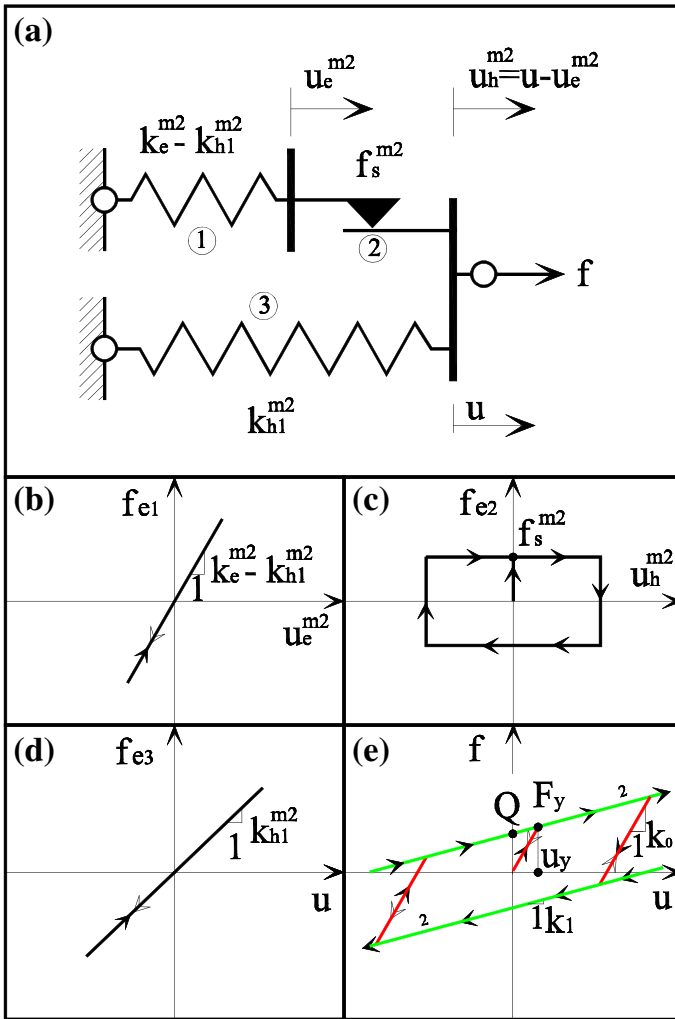


Fig. 2 Bilinear hysteretic model labeled BHM2: **a** mechanical model **b** $f_{e1}-u_e^{m2}$ graph of element 1 **c** $f_{e2}-u_h^{m2}$ graph of element 2 **d** $f_{e3}-u_h^{m2}$ graph of element 3 and **e** overall $f-u$ graph

change of slope in the spring from k_{h1}^{m2} to k_{h2}^{m2} and vice versa for positive displacements u , while the negative displacement $-u_c^{m2}$ denotes the change of slope between k_{h1}^{m2} and k_{h2}^{m2} for negative displacements u . The relationships between the parameters used in the mathematical models ($k_0, k_1, k_2, u_y, u_{yh}$) and those used in the corresponding mechanical ($k_e, k_{h1}, k_{h2}, u_c, f_s$) are presented in Table 1 for both THMs. Furthermore, the relationships between the mechanical parameters of the two systems are presented in Table 2, the compatibility equations are presented in Table 3, the equilibrium equations in Table 4 and finally the constitutive equations in Table 5. In the mathematical model, stiffness k_0 corresponds to the elastic phases, stiffness k_1 corresponds to plastic phase 2, and stiffness k_2 corresponds to plastic phases 1 and 3 (see Figs. 3 and 4). In the case of THM2, there is an additional elastic phase described by stiffness k_{01} . The yield displacement is denoted as u_y , the second

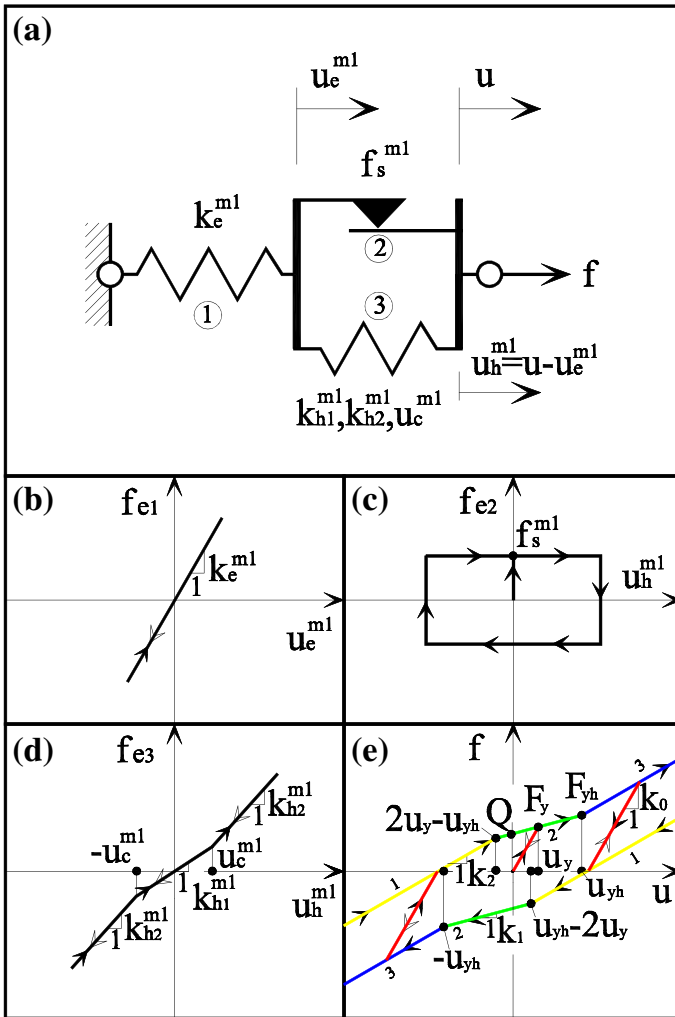


Fig. 3 Trilinear hysteretic model labeled THM1: **a** mechanical model **b** $f_{e1}-u_e^{m1}$ graph of element 1 **c** $f_{e2}-u_h^{m1}$ graph of element 2 **d** $f_{e3}-u_h^{m1}$ graph of element 3 and **e** overall $f-u$ graph

yield displacement is denoted as u_{yh} , the yield force at u_{yh} is denoted as F_{yh} , while the characteristic strength at zero displacement is denoted as Q and the yield force at u_y is denoted as F_y (see Figs. 3 and 4). In sum, both THMs are 5-parameter systems, see Tables 1 and 2.

The differences between the proposed two THMs are listed as follows:

- (i) THM1 exhibits three plastic phases (1, 2, 3) and one elastic phase with slope equal to $k_0 = k_e^{m1}$, see Fig. 3. On the other hand, THM2 also exhibits three plastic phases (1, 2, 3) and two elastic phases according to the displacement amplitude, see Fig. 4. For displacement amplitude smaller than u_{yh} in the THM2, the elastic phases are described by stiffness equal to $k_0 = k_e^{m2}$, while for displacement

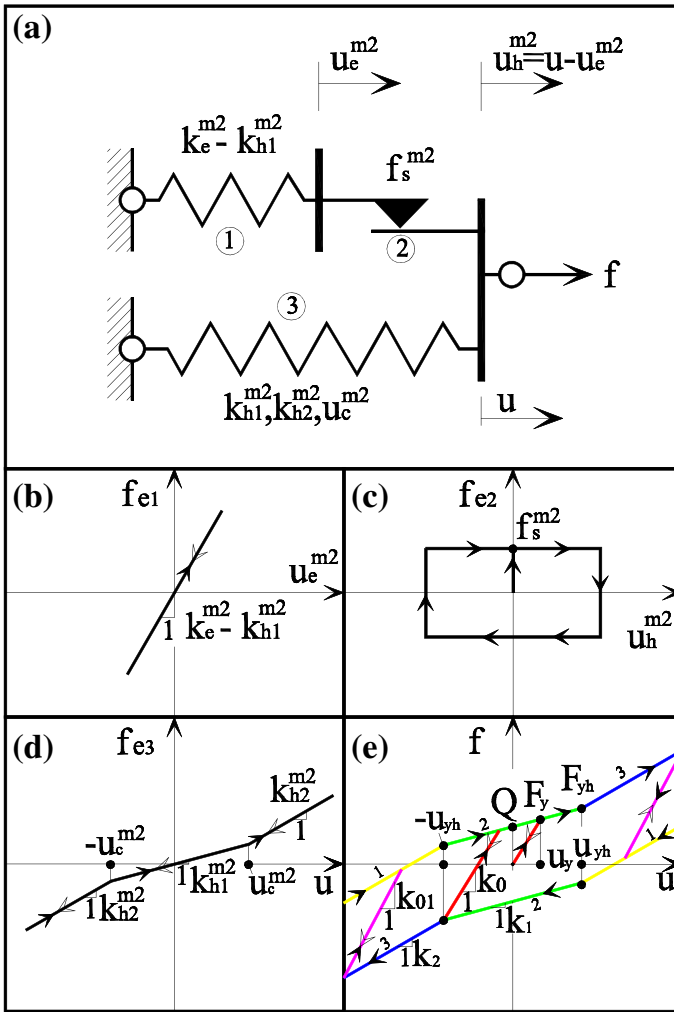


Fig. 4 Trilinear hysteretic model labeled THM2: **a** mechanical model **b** $f_{e1}-u_e^{m^2}$ graph of element 1 **c** $f_{e2}-u_h^{m^2}$ graph of element 2 **d** $f_{e3}-u_h^{m^2}$ graph of element 3 and **e** overall $f-u$ graph

Table 1 Relationships between mechanical and mathematical parameters of the THM1 and THM2 models

Model	THM1	THM2
k_e	k_0	k_0
k_{h1}	$k_1 \frac{k_0}{k_0 - k_1}$	k_1
k_{h2}	$k_2 \frac{k_0}{k_0 - k_2}$	k_2
f_s	$k_0 u_y = F_y$	$(k_0 - k_1) u_y = Q$
u_c	$(u_{yh} - u_y) \frac{k_0 - k_1}{k_0}$	u_{yh}
$k_e - k_{h1} + k_{h2}$	$k_0 \frac{k_0^2 - k_1(2k_0 - k_2)}{(k_0 - k_1)(k_0 - k_2)}$	k_{01}

Table 2 Relationships between the mechanical parameters of THM1 and THM2 models

THM1	k_e^{m1}	k_{h1}^{m1}	k_{h2}^{m1}	f_s^{m1}	u_c^{m1}
THM2	k_e^{m2}	$k_{h1}^{m2} \frac{k_e^{m2}}{k_e^{m2} - k_{h1}^{m2}}$	$k_{h2}^{m2} \frac{k_e^{m2}}{k_e^{m2} - k_{h2}^{m2}}$	$f_s^{m2} \frac{k_e^{m2}}{k_e^{m2} - k_{h1}^{m2}}$	$u_c^{m2} \frac{k_e^{m2} - k_{h1}^{m2}}{k_e^{m2}} - \frac{f_s^{m2}}{k_e^{m2}}$

Table 3 Compatibility equations of the THM1 and THM2 models

Model	THM1	THM2
u	$u_e^{m1} + u_h^{m1}$	$u_e^{m2} + u_h^{m2}$

Table 4 Equilibrium equations for the THM1 and THM2 models

Model	THM1	THM2
f	$f_{e1} = f_{e2} + f_{e3}$	$f_{e1} + f_{e3} = f_{e2} + f_{e3}$

Table 5 Constitutive equations for the THM1 and THM2 models

Model	THM1	THM2
f_{e1}	$k_e^{m1} u_e^{m1}$	$(k_e^{m2} - k_{h1}^{m2}) u_e^{m2}$
$f_{e2} (\dot{u}_h \neq 0)$	$f_s^{m1} \text{sgn}(\dot{u}_h^{m1})$	$f_s^{m2} \text{sgn}(\dot{u}_h^{m2})$
$f_{e2} (\dot{u}_h = 0)$	$f_{e1} - f_{e3}$	f_{e1}
$f_{e3} (u_h^* \leq u_c)$	$k_{h1}^{m1} u_h^{m1}$	$k_{h1}^{m2} u$
$f_{e3} (u_h^* > u_c)$	$(k_{h1}^{m1} u_c^{m1} + k_{h2}^{m1} (u_h^{m1} - u_c^{m1})) \text{sgn}(u_h^{m1})$	$(k_{h1}^{m2} u_c^{m2} + k_{h2}^{m2} (u - u_c^{m2})) \text{sgn}(u)$

* For THM2 replace u_h^* with u

amplitude larger than u_{yh} , the elastic phases are described by stiffness equal to $k_{01} = k_e^{m2} - k_{h1}^{m2} + k_{h2}^{m2}$, see Table 1, Fig. 4.

- (ii) The change of slope in the plastic phases in THM2 occurs at displacement u_{yh} for $u > 0$ and at $-u_{yh}$ for $u < 0$, see Fig. 4. In THM1, the change of slope in the plastic phases occurs at displacement u_{yh} for $u > 0$ and at $-u_{yh}$ for $u < 0$ during loading phases ($\dot{u}u > 0$), and at displacements $u_{yh} - 2u_y$ for $u > 0$ and at $2u_y - u_{yh}$ for $u < 0$ during the unloading phases ($\dot{u}u < 0$), see Fig. 3. In physical terms, the difference between the two THMs occurs because in THM1 element 3 is activated with displacement u_h , while in THM2 the same element 3 is activated by displacement u . Note that in the case of THM2 u_{yh} can be smaller than u_y , but in the case of THM1 u_{yh} can only be larger than u_y .
- (iii) The dissipated energy over a cycle of amplitude u_a is denoted as W_d in both THMs and presented in Table 6, where u_{ha} denotes the displacement u_h at displacement amplitude equal to u_a . Note that in order to have a dissipative system u_{ha} and subsequently W_d need to be positive. The energy dissipated over a cycle of motion of amplitude u_a by THM2 remains unaffected by the change of slope in the trilinear spring (element 3), as compared with the BHMs, see u_{ha} in Table 6. In the case of THM1, the energy is affected by the change of slope and does not remain the same as in BHMs. Let us assume that the energy dissipated in

Table 6 Energy dissipation over a cycle of amplitude u_a for the THM1 and THM2 models

Model	THM1	THM2
u_{ha}	$\frac{k_e^{m1} u_a - f_s^{m1} + u_c^{m1} (k_{h2}^{m1} - k_{h1}^{m1})}{k_e^{m1} + k_{h2}^{m1}}$	$u_a - \frac{f_s^{m2}}{k_e^{m2} - k_{h1}^{m2}}$
W_d	$4f_s^{m1} u_{ha}^{m1}$	$4f_s^{m2} u_{ha}^{m2}$

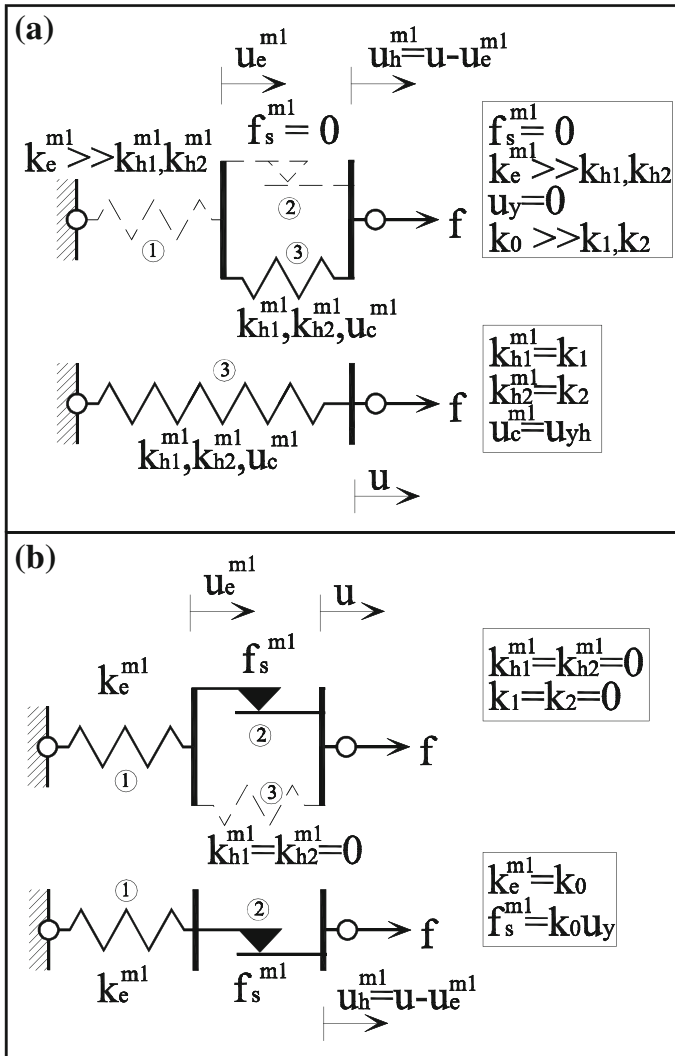


Fig. 5 Possible simplifications of THM1 model: **a** a trilinear elastic spring and **b** an elastoplastic element

Table 7 Parameters of the THM and BHM models for hardening and softening base isolation systems

Mathematical parameters							
	k_0 (kN/mm)	k_1 (kN/mm)	k_2 (kN/mm)	k_{01} (kN/mm)	u_y (mm)	u_{yh} (mm)	u_a (mm)
Hard	1	0.20	0.45	1.25	20	120	200
Soft			0.05	0.85			
Mechanical parameters							
	k_e (kN/mm)	k_{h1} (kN/mm)	k_{h2} (kN/mm)	f_s (kN)	u_c (mm)	u_{ha} (mm)	W_d (kNmm)
THM1							
Hard	1	0.25	0.819	20	80	124	9920
Soft			0.053			156	12480
THM2							
Hard	1	0.20	0.45	16	120	180	11520
Soft			0.05				

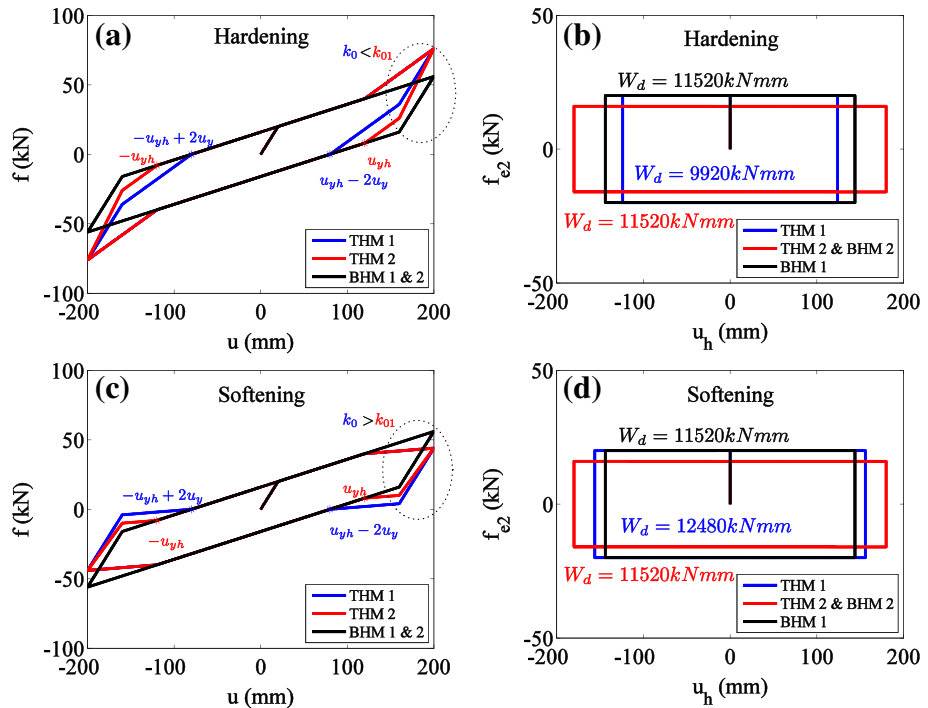


Fig. 6 Hysteretic model response force–displacement curves: **a** $f-u$, **b** $f_{e2}-u_h$ for hardening, **c** $f-u$, **d** $f_{e2}-u_h$ for softening

the THM1 is W_d^t at amplitude u_a and is larger than the dissipated energy in the BHM1 (W_d^b):

$$W_d^t > W_d^b \Leftrightarrow \frac{k_e^{m1}u_a - f_s^{m1} + u_c^{m1}(k_{h2}^{m1} - k_{h1}^{m1})}{k_e^{m1} + k_{h2}^{m1}} > \frac{k_e^{m1}u_a - f_s^{m1}}{k_e^{m1} + k_{h1}^{m1}} \tag{1}$$

Note that for the bilinear case $k_{h1}^{m1} = k_{h2}^{m1}$ and $u_{ha}^{m1} = \frac{k_e^{m1}u_a - f_s^{m1}}{k_e^{m1} + k_{h1}^{m1}}$. In order for THM1 to account for larger dissipated energy than the BHM1, the following inequalities need to be satisfied in terms of the mechanical and mathematical parameters, respectively:

$$(k_{h2}^{m1} - k_{h1}^{m1})(-k_e^{m1}(u_a - u_c^{m1}) + f_s^{m1} + k_{h1}^{m1}u_c^{m1}) > 0 \tag{2}$$

$$(k_1 - k_2)(u_a - u_{yh}) > 0 \tag{3}$$

For the THMs $u_a > u_{yh}$, implying that term $(u_a - u_{yh})$ is positive. In order for THM1 to account for larger energy dissipation as compared to BHM1, the following inequality must be satisfied:

$$k_1 > k_2 \tag{4}$$

The above inequality shows that the THM1 can describe larger amounts of energy dissipation in comparison with the BHM1, but only for softening cases ($k_1 > k_2$). In the

Table 8 Geometrical characteristics of the HDRB isolator

External diameter (mm)	500
Diameter of steel plates D (mm)	490
Thickness of steel plates (mm)	3
Number of rubber layers	12
Thickness of single rubber layer T_{ri} (mm)	8
Total rubber thickness T_r (mm)	96
Cross section area A_r (mm ²)	188574.10
Total height (mm)	169
Primary shape factor S_1	15.31
Secondary shape factor S_2	5.10

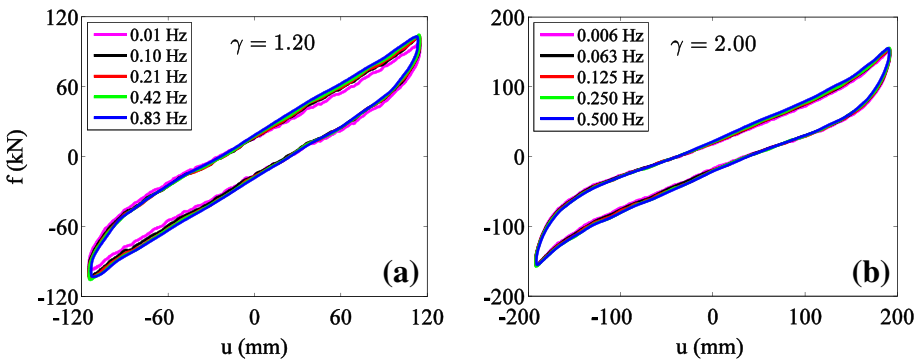
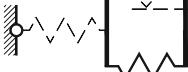
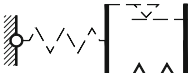
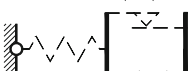








Fig. 7 Third cycle force–displacement graphs at different frequencies at shear strain amplitudes of **a** $\gamma = 1.20$ and **b** $\gamma = 2.00$

case of hardening ($k_1 < k_2$), the energy in THM1 decreases as compared to BHM1. This outcome can be explained physically, by realizing that the dissipation of all four systems (THM1, THM2, BHM1, BHM2) is related only to element 2, namely the plastic slider. As element 3 of THM1 becomes stiffer in the case of hardening, it allows for smaller displacements u_h in the plastic slider and therefore the dissipation of the system decreases. The opposite is true for the softening case. Note that in order for k_0 not to overlap either k_1 or k_2 , it needs to be larger than both, and then the system will be dissipative.

It is of interest to point out that each of the mechanical components of the THM2 is a particular case of the mechanical formulation of the THM1. More specifically, THM1 can

Table 9 Parallel mechanical system using the THM1 model components (33 parameters)

No.	Component	k_0 (kN/mm)	k_1 (kN/mm)	k_2 (kN/mm)	u_y (mm)	u_{yh} (mm)
1		$\gg k_1, k_2^a$	0.283532	0.489882	0 ^b	64.809
2		$\gg k_1, k_2^a$	0.000282	0.905635	0 ^b	136.491
3		$\gg k_1, k_2^a$	0.000246	0.877611	0 ^b	108.657
4		0.863754	0.402485	-0.792654	7.146	125.542
5		0.157047	0.000238	-0.285050	43.938	151.692
6		0.172839	0.000547	-0.271989	18.760	80.117
7		0.056183	0.044945	-0.006864	3.331	21.299
8		3.225241	0 ^c	0 ^c	0.597	- ^d
9		67.445070	0 ^c	0 ^c	0.041	- ^d
					e^2	2.50 %

^a Note that a very large value of $k_0 \gg k_1, k_2$ corresponds to a very stiff elastic spring, which can be neglected, see Fig. 5

^b Note that THM1 becomes a trilinear elastic spring for $u_y = 0$, see Fig. 5

^c Note that THM1 becomes an elastoplastic element for $k_1 = k_2 = 0$, see Fig. 5

^d Note that because $k_1 = k_2$, u_{yh} does not denote any change of stiffness, so it becomes meaningless

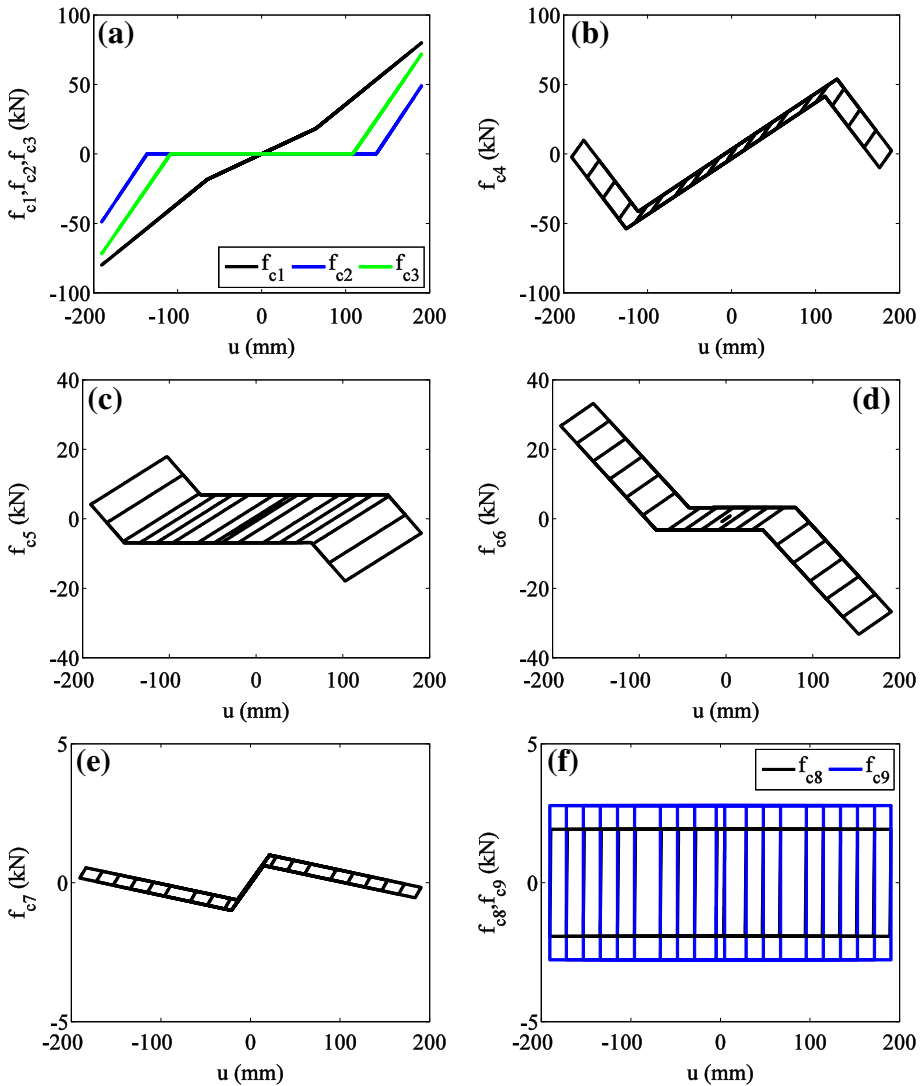


Fig. 8 Force–displacement curves of each separate component of the THM1 model for all strain amplitudes: **a** $f_{c1}-u, f_{c2}-u, f_{c3}-u$ graphs of elements 1,2,3 **b** $f_{c4}-u$ graph of element 4 **c** $f_{c5}-u$ graph of element 5 **d** $f_{c6}-u$ graph of element 6 **e** $f_{c7}-u$ graph of element 7 **f** $f_{c8}-u, f_{c9}-u$ graphs of elements 8,9

be simplified to a trilinear elastic spring for $f_s^{m1} = 0$ and $k_e^{m1} \gg k_{h1}^{m1}, k_{h2}^{m1}$ in terms of mechanical parameters and in terms of mathematical ones with $u_y = 0$ and $k_0 \gg k_1, k_2$, see Fig. 5a. In this case, element 1 of THM1 will be extremely stiff to account for any deformation and will be neglected, while element 2 will not account for any dissipation ($f_s^{m1} = 0$) and will also be neglected, so the system will behave linearly. The relation between mechanical and mathematical parameters (by taking into account that $\frac{k_0}{k_0-k_1} \simeq \frac{k_0}{k_0-k_2} \simeq \frac{k_0-k_1}{k_0} \simeq 1$, see Table 1) is the following: $k_{h1}^{m1} = k_1, k_{h2}^{m1} = k_2$ and $u_c^m = u_{yh}$, which results to a three-parameter system.

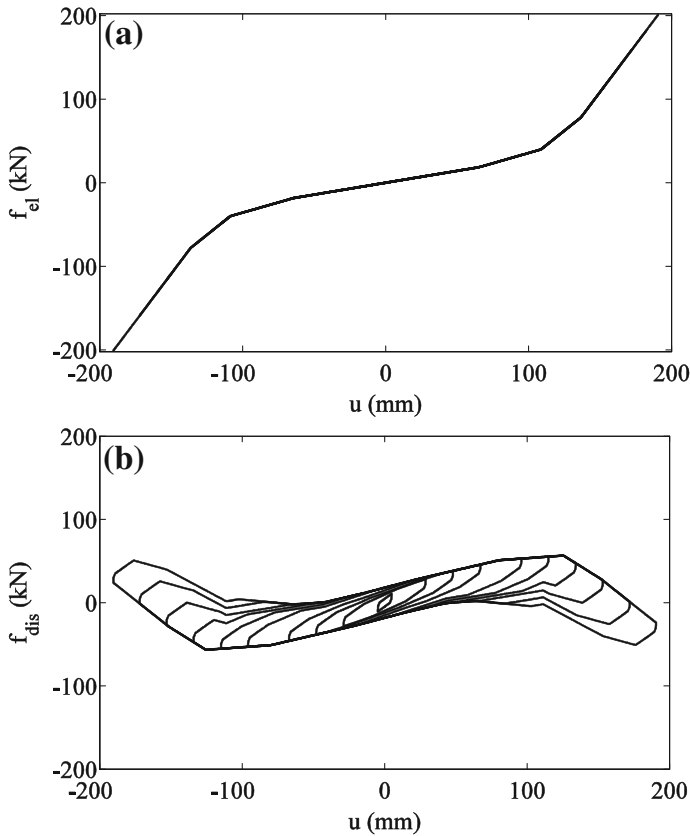


Fig. 9 **a** Elastic and **b** dissipative force breakdown in the THM1 model

Let us now consider the stiffnesses of element 3 of the THM1 to be zero, namely $k_{h1}^{m1} = k_{h2}^{m1} = 0$ and in mathematical terms $k_1 = k_2 = 0$, see Fig. 5b. In this case, the THM1 will behave like any elastoplastic element and the relation between mechanical and mathematical parameters will be $k_e^{m1} = k_0$ and $f_s^{m1} = k_0 u_y$ (see Table 1) which results in a two-parameter system. Note that characteristic displacement u_c^{m1} becomes meaningless because $k_{h1}^{m1} = k_{h2}^{m1}$.

3 Numerical implementation

Two different sets of parameters are used as examples in order to quantify the differences between the previously described mechanical formulations. The first one accounts for hardening ($k_1 < k_2$) and the second one for softening ($k_1 > k_2$). The parameters of the mathematical model, along with the mechanical parameters of the two formulations, are given in Table 7. The only difference in the mathematical parameters between the hardening case and the softening one is the change of k_2 from 0.45 kN/mm to 0.05 kN/mm, which also affects k_{01} . Two cycles of harmonic displacement of amplitude $u_a = 200$ mm are imposed in the systems and the energy of the complete second cycle W_d is calculated

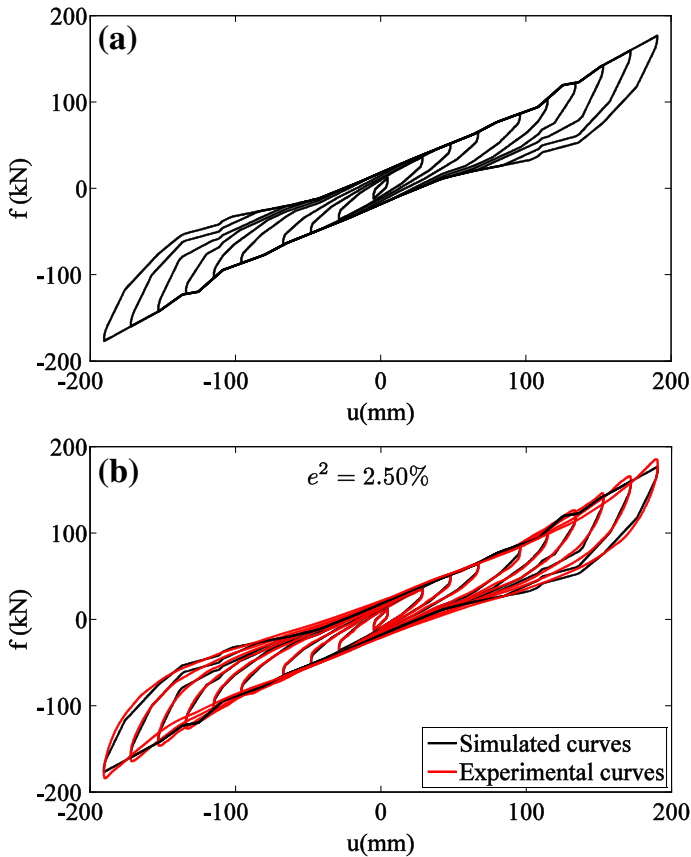


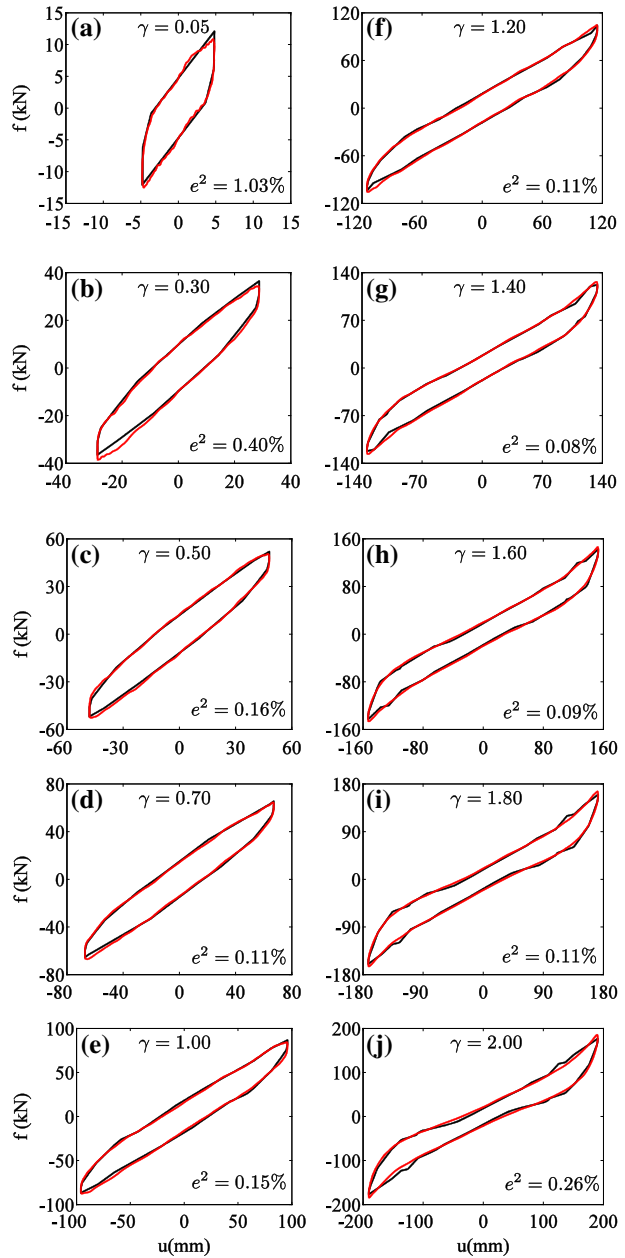
Fig. 10 **a** Force-displacement curves of the THM1 model and **b** comparison of the numerically simulated with the experimental results

along with u_{ha} , see Table 7. In Fig. 6, the $f - u$ and $f_{e2} - u_h$ relationships are plotted for hardening and softening cases for both THMs and BHMs. As shown in Fig. 6a and c, the change of slopes in the plastic phases does not occur at the same displacement value for THM1 and THM2 during the unloading phases ($u\dot{u} < 0$). In the same figures, it is seen that the elastic stiffness k_{01} of THM2 for the elastic phases at displacements $|u| > u_{yh}$, is larger than k_0 for the hardening case and smaller for the softening one. Finally, Fig. 6b–d show that the dissipated energy W_d increases for the THM1 for softening, decreases for hardening, while it remains unchanged for THM2 and equal to the dissipated energy in both BHM1 and BHM2.

4 Parameter identification using cyclic shear tests on HDRB

In this section the third cycle of a set of cyclic shear tests that were conducted on a HDRB from the Solarino project ten years later in the laboratories of the University of Basilicata in Italy (Markou et al. 2014) will be used for the parameter identification using different parallel systems comprising either THM1 or THM2. The geometrical characteristics of the







Fig. 11 Identification of the force–displacement curves of THM1 model by using the third cycle of harmonic tests at ten different strain amplitudes and at a frequency 0.5 Hz under compressive stress of 6 MPa: **a** $\gamma = 0.05$ **b** $\gamma = 0.30$ **c** $\gamma = 0.50$ **d** $\gamma = 0.70$ **e** $\gamma = 1.00$ **f** $\gamma = 1.20$ **g** $\gamma = 1.40$ **h** $\gamma = 1.60$ **i** $\gamma = 1.80$ **j** $\gamma = 2.00$ (black color indicates numerical simulations and red color denotes the experimental data)



HDRB are given in Table 8. The cyclic shear tests were conducted under a compressive stress of 6MPa at a frequency 0.5Hz for ten different strain amplitudes varying from $\gamma = 0.05$ to $\gamma = 2$.

Apart from the cyclic shear tests, cyclic tests at different strain amplitudes ($\gamma = 1.20$ and $\gamma = 2.00$) at variable frequencies (from 0.006 Hz to 0.83 Hz) were implemented to investigate the effect of rate-dependence of the bearings, see Fig. 7. The devices can be

Table 10 Parallel mechanical system using the THM2 model components (30 parameters)

No.	Component	k_0 (kN/mm)	k_1 (kN/mm)	k_2 (kN/mm)	u_y (mm)	u_{yh} (mm)
1		3.316369	0.097634	0.066989	0.604	34.120
2		67.826800	0.034459	0.242161	0.041	181.563
3		0.583996	0.082570	0.258475	7.945	102.741
4		0.360200	0.159367	0.287472	128.456	139.534
5		0.315248	0.115504	0.225922	20.728	99.702
6		0.142166	0.010595	0.325443	43.731	162.318
					e^2	5.00 %

assumed as rate independent in the range of frequencies of interest under seismic excitation.

To this end, two different rate-independent parallel systems are used to describe the cyclic shear tests, one comprising THM1 and the other THM2. The identification procedure that was used for the definition of the parameters is the CMA-ES algorithm developed by Hansen (2011). In Table 9 the identified mathematical parameters of the THM1 system are presented along with the corresponding mechanical formulations. The identification error e^2 , also shown in Table 9, is defined as follows:

$$e^2 = \sum_{i=1}^{10} \frac{\langle F_{0i} - \tilde{F}_i, F_{0i} - \tilde{F}_i \rangle}{\langle F_{0i}, F_{0i} \rangle} \tag{5}$$

where F_{0i} and \tilde{F}_i are the measured and computed force vectors at ten different strain amplitudes, and

$$\langle A, B \rangle = \sum_{i=1}^n A_i B_i \tag{6}$$

is the standard inner vector product.

Nine THM1 components are connected in parallel to describe the shear behavior of the device, but some of them represent simplified versions of THM1 as was pointed out in

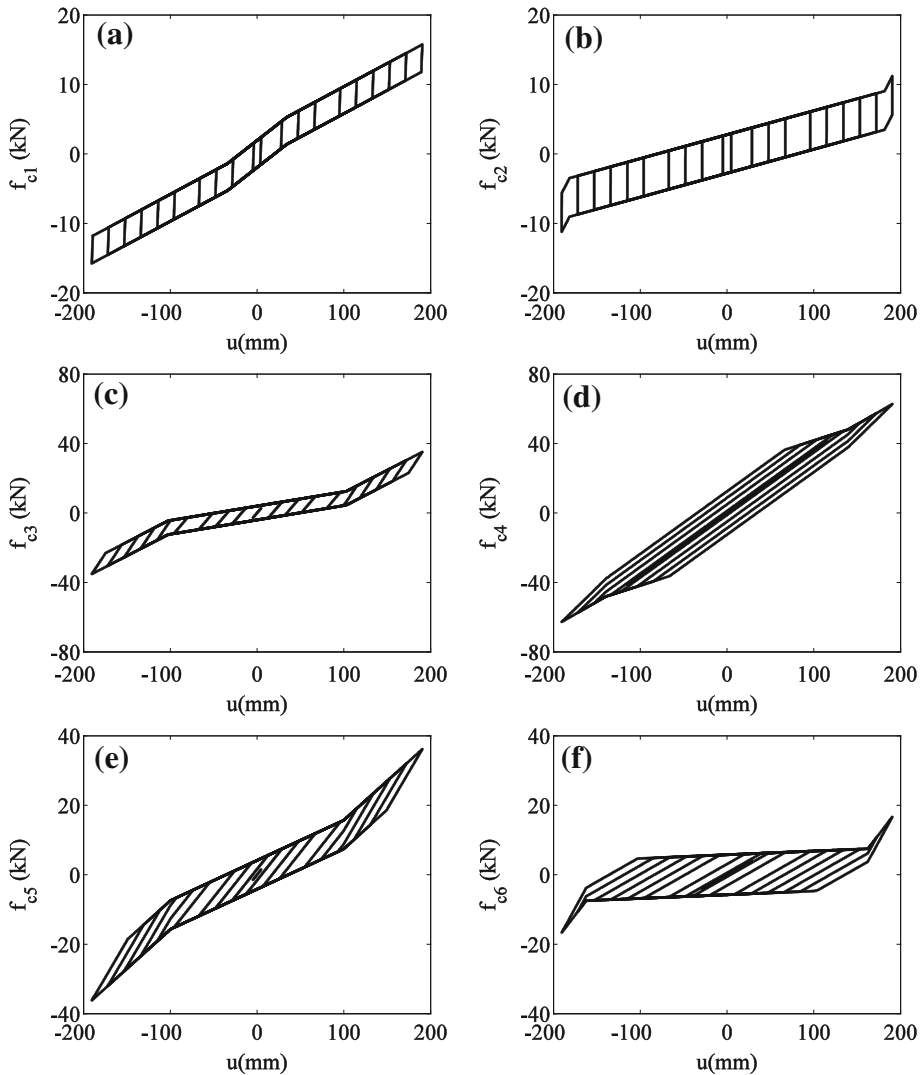


Fig. 12 Force–displacement curves for each component of the THM2 model for all strain amplitudes: **a** $f_{c1}-u$ graph of element 1 **b** $f_{c2}-u$ graph of element 2 **c** $f_{c3}-u$ graph of element 3 **d** $f_{c4}-u$ graph of element 4 **e** $f_{c5}-u$ graph of element 5 **f** $f_{c6}-u$ graph of element 6

Fig. 5. Specifically, we have the trilinear elastic spring (components 1, 2 and 3) and the elastoplastic element (components 8 and 9).

It may be of interest to note that trilinear elastic springs (components 1, 2 and 3) are hardening springs ($k_2 > k_1$) accounting for the hardening behavior of the device at higher strain amplitudes, see Table 9 and Fig. 8a. On the other hand, components 4, 5, 6 and 7 give softening behavior ($k_2 < k_1$), while in all of these cases k_2 is negative, see Table 9 and Fig. 8b–e. These four components are responsible for describing the enlargement of the dissipated energy as the strain amplitude increases. The combination of the hardening

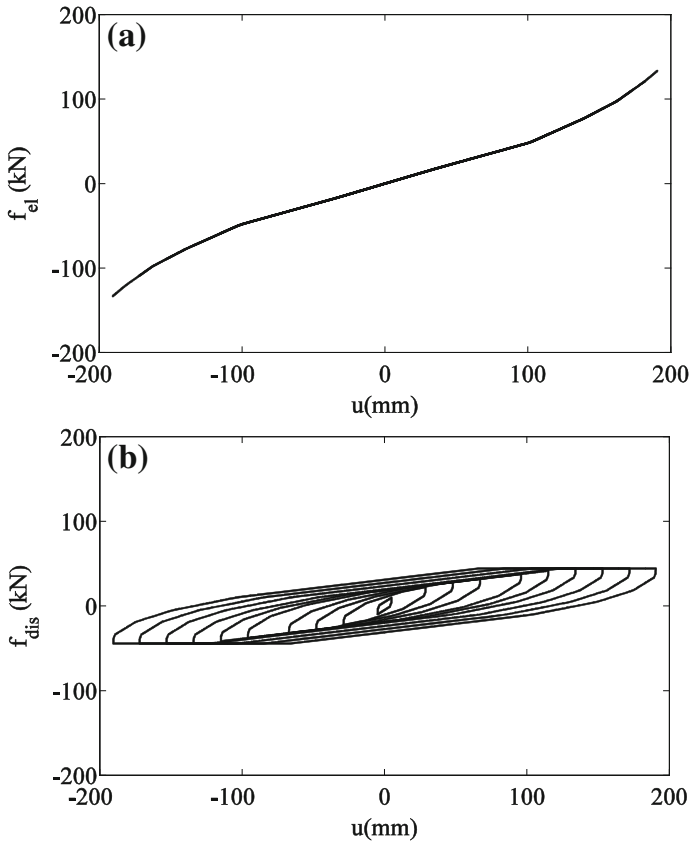


Fig. 13 a Elastic and b dissipative force breakdown in the THM2 model

trilinear elastic springs and the softening trilinear hysteretic systems provides a better description of the changing behavior during the loading ($u\dot{u} > 0$) and unloading ($u\dot{u} < 0$) paths, as was pointed out in Markou and Manolis (2016b). Also, Fig. 9 should be consulted, where the elastic and dissipative contributions of the components of the THM1 system are presented. Additionally, elastoplastic elements (components 8 and 9) are responsible to describe the energy dissipation for small strain amplitudes due to their small yield displacement u_y , see Table 9 and Fig. 8f. Next, Fig. 10 presents the overall behavior of the THM1 system for all strain amplitudes along with the comparison against the experimental results. Finally, Fig. 11 gives a better representation of the comparison of the THM1 system with the experimental results at each strain amplitude separately, and clearly shows an almost perfect fit between simulated and recorded curves. The total number of parameters for the THM1 system is 33 and the identification error is rather small at $e^2 = 2.50\%$.

Six THM2 components are connected in parallel to describe the shear behaviour of the HDRB experiment, and the identified mathematical parameters are presented in Table 10, along with the corresponding mechanical formulations. Component 1 has softening behavior ($k_2 < k_1$), while the remaining components show hardening behavior ($k_2 > k_1$),

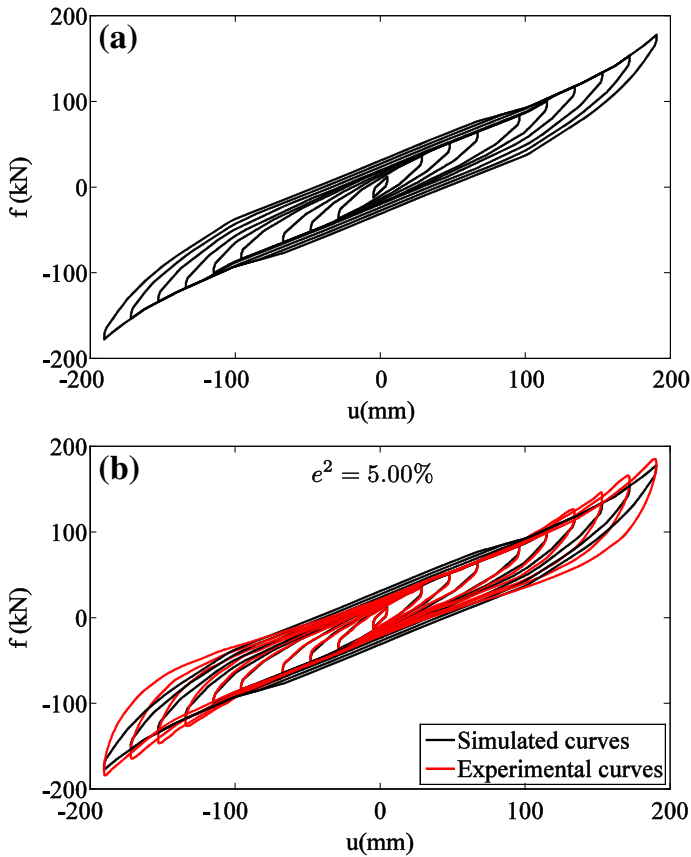


Fig. 14 **a** Force-displacement curves of the THM2 model and **b** comparison of the numerically simulated with the experimental results

see Table 10 and Fig. 12. Components 1 and 2 have a small yield displacement u_y , and they describe the energy dissipation for small strain amplitudes, where the rest of the components remain in the elastic range. In Fig. 13, the elastic and dissipative contributions of the THM2 system are presented, while in Fig. 14 the overall behavior of the THM2 system is presented along with the comparison with experimental data. The comparison shows that the system fails to describe the larger energy dissipation at larger strain amplitudes. The total number of parameters of the THM2 system is 30, and the identification error is $e^2 = 5.00\%$, namely twice that of the THM1 system. Additional THM2 components did not help improve the fitting between experimental and simulated curves, meaning that six THM2 is the limit for this case.

For more details on the modelling approach for the THM1 the reader is referred to Markou et al. (2016), where the THM1 is solved analytically for the case of the single degree of freedom systems, while ongoing work aims to develop numerical implementation for the case of multi-degree of freedom systems. For the case of THM2, the system can be solved by using Newmark's method combined with Newton–Raphson iteration, see Chopra (2012).

5 Conclusions

Two different mechanical formulations corresponding to the same basic mathematical model for the well-known BHM are introduced here. In order to account for hardening and softening effects observed in various materials and structural components, the extension of each BHM, which now becomes a THM, is presented. The differences between the two possible THMs (models 1 and 2), in terms of both mechanical and mathematical representations, are highlighted and explained. More specifically the differences are: (a) THM1 exhibits three plastic phases and one elastic phase, while THM2 exhibits three plastic phases and two elastic phases; (b) the change of slope in the plastic phases during unloading ($\dot{u} < 0$), does not occur at the same displacement level for either model; and (c) the dissipated energy per cycle of amplitude u_a decreases in the case of hardening and increases in the case of softening for the THM1 model, while in THM2 model the dissipated energy remains constant as is the case with the BHMs and it is not affected by either softening or hardening effects. Next, numerical applications are presented in order to quantify these differences observed in the behaviour of the two THMs. A set of cyclic shear tests on a HDRB under a wide range of strain amplitudes shows that the shear behaviour observed can be described by a parallel system, which comprises only one type of component, namely the THM1 with identification error $e^2 = 2.50\%$. On the other hand, a parallel-type THM2 model fails to describe the behaviour of the HDRB since it does not account for increasing energy dissipation at larger amplitudes (the identification error here is $e^2 = 5.00\%$). Compared to THM2, THM1 has the following advantages: (a) it accounts for larger energy dissipation at larger strain amplitudes; (b) it better describes the different behaviour observed during the loading ($\dot{u} > 0$) and unloading ($\dot{u} < 0$) paths in the HDRB; and (c) the THM1 mechanical model, through a proper choice of parameters, can be reduced to simpler models, namely a trilinear elastic spring and an elastoplastic element, which actually are the two mechanical components of the THM2 model.

Acknowledgments This work was financially supported by the Greek Secretariat for Research and Technology (GSRT) Thales Project entitled “Antiseismic Protection of Monuments and Historic Structures”, Prof. C.C. Spyarakos, Principal Investigator, National Technical University of Athens, 2010–2014. The authors also wish to acknowledge the assistance of Prof. G. Oliveto, University of Catania, through project ReLUIIS (Italian National Network of University Earthquake Engineering Laboratories), and projects D.P.C-ReLUIIS 2014–2016, Profs. F.C. Ponzio and G. Serino, Coordinators and Horizon 2020 MSCA-RISE-2015 project No. 691213 entitled “Exchange-Risk”, Prof. A. Sextos, Principal Investigator.

References

- Besson J, Cailletaud G, Chaboche JL, Forest S, Bletry M (2010) Non-linear mechanics of materials. Springer, Heidelberg
- Chopra AK (2012) Dynamics of structures, Theory and Applications to Earthquake Engineering. Prentice Hall, Boston
- Hansen N (2011) The CMA evolution strategy: a tutorial. <https://www.lri.fr/~hansen/cmatutorial.pdf>
- Ibarra LF, Medina RA, Krawinkler H (2005) Hysteretic models that incorporate strength and stiffness deterioration. Earthq Eng Struct Dyn 34(12):1489–1511
- Iwan WD (1961) The dynamic response of bilinear hysteretic systems, PhD dissertation, California Institute of Technology, Pasadena, California
- Markou AA, Manolis GD (2016a) A fractional derivative Zener model for the numerical simulation of base isolated structures. Bull Earthq Eng 14(1):283–295
- Markou AA, Manolis GD (2016b) Mechanical models for shear behavior in high damping rubber bearings. Soil Dyn Earthq Eng 90:221–226

- Markou AA, Oliveto G, Mossucca A, Ponzo FC (2014) Laboratory experimental tests on elastomeric bearing from the Solarino project. Progetto di Ricerca DPC–RELUIS, Linea di Ricerca 6: Isolamento e Dissipazione, Coordinatori: Ponzo FC and Serino G, University of Basilicata, Italy
- Markou AA, Oliveto G, Athanasiou A (2016) Response simulation of hybrid base isolation systems under earthquake excitation. *Soil Dyn Earthq Eng* 84:120–133
- Oliveto G, Oliveto ND, Athanasiou A (2014) Constrained optimization for 1-D dynamic and earthquake response analysis of hybrid base-isolation systems. *Soil Dyn Earthq Eng* 67:44–53
- Ozdemir H (1976) Nonlinear transient dynamic analysis of yielding structures, PhD dissertation, University of California, Berkeley, California
- Ray T, Reinhorn AM (2013) Enhanced smooth hysteretic model with degrading properties. *J Struct Eng* 140(1):04013028
- Ray T, Sarlis AA, Reinhorn AM, Constantinou MC (2013) Hysteretic models for sliding bearings with varying frictional force. *Earthq Eng Struct Dyn* 42(15):2341–2360
- Tsopelas PC, Constantinou MC, Reinhorn AM (1994) 3D-BASIS-ME: computer program for nonlinear dynamic analysis of seismically isolated single and multiple structures and liquid storage tanks, NCEER-94-0010. Multidisciplinary Center for Earthquake Engineering Research, University at Buffalo, New York
- Wen YK (1976) Method for random vibration of hysteretic systems. *J Eng Mech ASCE* 102:249–263